1.10 Entrainment

When a dense layer of fluid spills over a sill and accelerates, the shear between the moving layer and the overlying fluid increases. These conditions favor the formation of shear instabilities and turbulent mixing about the interface. Turbulence in the bottom boundary layer can also intensify and sometimes penetrate up to the interface. In cases where the turbulence is localized near the level of the interface, the mixing gives rise to an intermediate region whose thickness increases with downstream distance. A numerical simulation of this process is shown in Figure 1.10.1. The flow upstream of the obstacle consists of homogeneous upper and lower layers separated by a thin region of rapidly varying stratification (upper panel). The upper layer is relatively quiescent but the lower layer flows towards the obstacle and spills over the sill in a familiar way. Downstream of the sill the interfacial region thickens and eventually spreads to the bottom. The streamlines in the upper fluid (bottom panel) suggest a slow subduction of fluid into the dense overflow.

Following ideas discussed by Gerdes *et al*. (2002), it is possible to formulate a model for the lower layer that incorporates turbulent mixing but retains the layer formalism. Consider an idealization of the intermediate region as typically produced in laboratory experiments (Figure 1.10.2). Two homogeneous layers of different density and velocity are brought into contact at the left-hand boundary. Mixing between the two results in the formation of a wedge-like intermediate region. Suppose that all of the fluid lying below the upper boundary of the wedge is treated as a single layer. Then the effect of mixing is to cause upper layer fluid to be *entrained* into this lower layer. Should the interface be defined to coincide with the lower boundary of the wedge, the lower layer fluid would be *detrained*. In the first scenario, the mass flux in the lower layer increases with downstream distance; in the second scenario it decreases. The loss or gain of fluid by a particular layer can be accounted for by introducing an *entrainment velocity* w_e that is normal to the interface and that carries fluid parcels, and the properties of those parcels, across the interface. Since the shallow water model assumes the interface to be nearly horizontal, the entrainment velocity is nearly vertical and will be approximated as such. We will concentrate on the process of entrainment as depicted in Figure 1.10.1. By convention, w_e is positive in the direction of entrainment, here downwards.

A second assumption required to retain the layer-model formalism is that the entrained mass and momentum are instantly mixed all the way to bottom, so that the lower layer density and velocity depend only on y (Figure 1.10.2b). The resulting 'slab' model is most convincing when the interfacial or bottom-generated turbulent eddies are comparable in size to the layer thickness. With these idealizations, the equations of volume and mass conservation for a one-dimensional lower layer are

$$\frac{\partial(v_2 d_2)}{\partial y} = w_e \tag{1.10.1}$$

and

$$\frac{\partial(\rho_2 v_2 d_2)}{\partial y} = w_e \rho_1 . \tag{1.10.2}$$

The subscripts 1 and 2 denote the upper and lower layer, respectively, and the width of the channel is assumed constant. If the first equation is multiplied by ρ_1 and subtracted from the second equation, it follows that $(\rho_2(y) - \rho_1)v_2 d_2$ is independent of *y*. A more common form for this quantity is the *buoyancy flux* $g' v_2 d_2$, where $g'(y) = (\rho_2(y) - \rho_1)/\rho_1$.

The entrainment process carries momentum from the overlying fluid into the lower layer and consequences for the lower layer momentum equation must be dealt with carefully. Consider a control volume drawn about a column of lower layer fluid extending from the bottom to the interface, as shown in Figure 1.10.3. The sum of the horizontal forces acting on the four faces of the volume must equal the sum of the fluxes of horizontal momentum into the volume. Thus

$$\int_h^{h+d_2} (\rho_2 v_2^2 + p_2)\Big|_{y+dy} dz - \int_h^{h+d_2} (\rho_2 v_2^2 + p_2)\Big|_y dz \cong p\big|_{h+d} \frac{\partial(h+d_2)}{\partial y} dy - p\big|_h \frac{\partial h}{\partial y} dy + w_e \rho_1 v_1 dy$$

The terms on the left hand side are the integrals over the left and right control volume faces of the momentum flux and pressure force. The first two terms on the right hand side represent first-order approximations to the horizontal component of the pressure force exerted at the top and bottom surfaces of the control volume. The final term represents the flux of horizontal momentum across the interface by the entrainment velocity. Dividing the above relation by *dy* and taking *dy*→0 results in the differential relation

$$\frac{\partial}{\partial y}\int_h^{h+d_2} (\rho_2 v_2^2 + p_2) dz \cong p\big|_{h+d} \frac{\partial(h+d_2)}{\partial y} - p\big|_h \frac{\partial h}{\partial y} + w_e \rho_1 v_1 . \tag{1.10.3}$$

The integral of $\rho_2 v_2^2$ is just $d_2 \rho_2 v_2^2$ and the derivative of the pressure integral can be written as $\int_h^{h+d_2} \frac{\partial p_2}{\partial y} dz + p_{h+d_2} \frac{\partial(h+d_2)}{\partial y} - p_h \frac{\partial h}{\partial y}$, the final two terms of which negate identical terms on the right hand side of (1.10.3). With these modifications, (1.10.3) reduces to

$$\frac{\partial}{\partial y}(\rho_2 d_2 v_2^2) + \int_h^{h+d_2} \frac{\partial p}{\partial y} dz = w_e \rho_1 v_1 \tag{1.10.4}$$

The integral can be evaluated by calculating the hydrostatic pressure in the lower layer, an exercise left to the reader. It is here that the inactive character of the upper layer is enforced. The upper layer depth is assumed to be so much greater than d_2 that the pressure at the rigid lid ($z=z_T$) and the upper layer velocity v_1 remain constant. Equation (1.10.4) now becomes

$$\frac{\partial}{\partial y}\left[\rho_2 d_2 v_2^2 + g(\rho_2-\rho_1)\frac{d_2^2}{2}\right] = -(\rho_2-\rho_1)gd_2\frac{dh}{dy} + w_e\rho_1 v_1 \qquad (1.10.5)$$

In this 'flux' form of the momentum equation, a generalization of (1.6.11) the flow 'force' $\rho_2 d_2 v_2^2 + g(\rho_2-\rho_1)\frac{d_2^2}{2}$ can only be altered by bottom pressure drag or by fluxes of horizontal momentum across the interface.

In order to investigate the effects of entrainment on the hydraulic properties of the flow, it is convenient to work with the equation for horizontal momentum per unit mass. We assume that $(\rho_2-\rho_1)/\rho_2 << 1$ and apply the Boussinesq approximation, meaning that density variations of $0[(\rho_2-\rho_1)/\rho_2]$ are ignored unless multiplied by g (also see Section 5.1). Expansion of the y-derivative of the terms on the right, division the result by d_2, and use of (1.10.1) and (1.10.2) leads to the modified momentum equation:

$$v_2\frac{\partial v_2}{\partial y} + g'\frac{\partial d_2}{\partial y} = -g'\frac{dh}{dy} + w_e\frac{(v_1-v_2)}{d_2} + g'\frac{w_e}{2v_2}. \qquad (1.10.6)$$

The interfacial flux of horizontal momentum per unit mass is proportional to the difference in layer velocities. If the upper layer is at rest (v_1=0), the corresponding term reduces to $-w_e v_2/d_2$. The second entrainment term ($g'w_e/2v_2$)has a more a subtle interpretation. It originates from the y-derivative of $g\rho_2(y)$ in (1.10.5), leading to $\frac{1}{2}gd_2^2\partial\rho_2/\partial y$, the contribution to the pressure gradient due to variations of the lower layer density. [Use of (1.10.1) and (1.10.2) allows this term to be rewritten in the form that appears in (1.10.6).] The entrainment of upper layer fluid causes the lower layer density to decrease in the direction of flow. In terms of pressure, the effect is the same as if the interface elevation decreased in the direction of flow.

As discussed by Pedlosky (1996, Sec. 4.2) there is an alternate model for w_e that holds in cases of thermal forcing. Direct cooling is imagined to trigger a convection process in which the density of an upper layer parcel increase from ρ_1 to ρ_2, causing it to sinks across the interface. In this setting the lower layer density is preserved and the final term in (1.10.6) is absent.

Some of the effects of entrainment on hydraulic properties are revealed by consideration of the evolution of the Froude number of the flow:

$$\frac{\partial F_d^{\,2}}{\partial y} = \frac{\partial}{\partial y}\left(\frac{v_2^2}{g' d_2}\right) = F_d^{\,2}\left[\frac{2}{v_2}\frac{\partial v_2}{\partial y} - \frac{1}{d_2}\frac{\partial d_2}{\partial y} - \frac{1}{\rho_2 - \rho_1}\frac{\partial \rho_2}{\partial y}\right]$$
$$= \frac{3F_d^{\,2}}{(F_d^{\,2}-1)d_2}\left\{-\frac{dh}{dy} + \frac{w_e}{v_2}(F_d^{\,2}\frac{v_1}{v_2} - F_d^{\,2} - \tfrac{1}{2})\right\} \qquad (1.10.7)$$

This relation was first derived by Gerdes, *et. al*. (2002), who also show that inclusion of width variations and quadratic bottom drag adds the term

$$-\frac{F_d^{\,2}}{F_d^{\,2}-1}[\frac{3F^2C_d}{d_2} - \frac{(2+F_d^{\,2})}{W}\frac{dW}{dy}]$$

to the right hand side.

Generalizations are straightforward for the case in which the velocity of the upper layer is less than or equal to that of the lower layer ($v_1/v_2 \leq 1$). In this case, the entrained momentum flux tends to retard the flow. Then the terms proportional to w_e in (1.19.12) make a positive contribution to $\partial F_d^{\,2} / \partial y$ when the flow is subcritical and a negative contribution when the flow is supercritical. In this case, entrainment drives the flow towards a critical state. It also tends to shift the point of hydraulic control downstream of the sill, to a location given by

$$\frac{dh}{dy} = \frac{w_e}{v_2}\left(\frac{v_1}{v_2} - \frac{3}{2}\right). \qquad (1.10.8)$$

If entrainment adds momentum to the flow ($v_1 > v_2$) it is harder to make generalizations. However, (1.19.13) does show that entrainment will move the control section to a point upstream of a sill provided the value of v_1/v_2 exceeds 3/2. This shift would only occur if mixing (and corresponding finite values of w_e) occurred upstream of the sill.

A standard parameterization for the entrainment velocity is that due to Ellison and Turner (1959):

$$w_e = \begin{cases} |v_1 - v_2|\left(\dfrac{0.08 - 0.1R_i}{1+5R_i}\right) & (R_i < 0.8) \\ 0 & (R_i \geq 0.8) \end{cases}, \qquad (1.10.9)$$

where

$$R_i = F_d^{-2}\left(\frac{v_1}{v_2} - 1\right)^{-2}.$$

is called the *bulk Richardson number*. If the upper layer is motionless (v_1=0) then F_d=R_i^{-2} and the requirement R_i<0.8 means that entrainment only occurs for supercritical flows.

In our formulation of the shallow water equations with entrainment, w_e is considered to be a vertical velocity. In ocean overflows, where outflow bottom slopes are of the order 10^{-2} or smaller, this approximation is justified. In the Ellison-Turner formulation, and in other situations involving a non-negligible interface tilts, w_e is considered to be directed normal to the interface. The Froude number in such cases is based on the velocity component parallel to the bottom and on the layer thickness measured normal to the bottom. In some of these cases, the interface more or less parallels the bottom and w_e is then taken to be normal to the bottom.

One consequence of using a large bottom slope in an experiment is that the Froude numbers obtained tend to be larger than those observed in the ocean (Figure 1.10.4). The entrainment rates also tend to be unrealistically large. Recent experiments (e.g. Cenedese *et al*. 2004) designed to achieve lower Froude numbers have reproduced more realistic entrainment rates. Estimates of w_e for the outflows of the Mediterranean, the Denmark Strait, and the Faroe-Bank Channel, as well as a dense gravity plume in Lake Ogawara, are shown in the figure along with data from three laboratory experiments. The entrainment velocity in the low Froude number, oceanographically relevant range increases roughly in proportion to the eighth power of the Froude number (Price, *private communication*, solid line). The shaded areas in the figure correspond to laboratory studies and the symbols to geophysical data from oceans and lakes.

There are also examples of measurements in the atmosphere (e.g. Princevac *et al*. 2004) involving flows with oceanic Froude numbers but comparatively large Reynolds numbers. The turbulence in such cases is more fully developed and the entrainment rates are larger (upper left data points in Figure 1.10.4). A parameterization based solely on the Froude number is clearly inadequate to explain all cases. Another questionable practice in the formulation of parameterizations of turbulence, here and at large, is the reliance on local properties of the background flow. Turbulent eddies generated at a particular location may intensify or grow as they are advected by the mean velocity field. The value of w_e at a certain y may therefore depend on the background flow at and upstream of that y.

If the Ellison-Turner parameterization is used to specify w_e, the resulting solutions (Figures 1.10.5 and 1.10.6) show some of the features anticipated earlier in this discussion. The solutions are obtained by fixing the upstream values of v_2d and g' and varying the upstream value of d. Equations (1.10.1), (1.10.2) and (1.10.7) are then integrated forward in y to obtain the solutions at points downstream. The solutions should be compared to the conservative family of solutions shown in Figure 1.7.3. When the upper layer is motionless (v_1=0, Figure 1.10.5), w_e is finite only when the Froude number exceeds unity. In this case the subcritical solution (upper solid curve in Frame a) is unaffected. On the other hand, the supercritical (dashed) solutions are greatly altered. For example, the solution with upstream depth d(-3)=0.05 immediately experiences entrainment causing its volume flow rate and depth to rapidly increase over much of the domain. The depth (≅4.0) that this solution reaches at the downstream end of the domain is greater than all other solutions shown, despite the fact that its upstream depth is less than all the other solutions.

Critical flow at the sill is obtained when the upstream flow is subcritical and has value $d(-3)\cong 2.41$ or when the upstream flow is supercritical and has value $d(-3)\cong 0.26$. In each case, the subcritical and supercritical branches of the solution that occur downstream of the critical section are shown. The appropriate choice of downstream solution is the one that allows the fluid to pass smoothly through the critical section. For example, one would follow the subcritical (solid) curve beginning at $d(-3)\cong 2.41$ and continue on to the supercritical (dashed) branch downstream of the sill. (There is an upstream continuation of the downstream subcritical branch, however this solution is associated with different upstream values of $v_1 d$ and g' than those used to generate the family of curves in Figure 1.10.5).

Intersections between different solution curves do not carry the same significance as in a conservative system. In the latter, intersections imply the existence of two solutions with the same depth and volume fluxes, but different interface slopes. Such behavior is indicative of critical flow since it implies that stationary disturbances can exist at the section in question. An example is the intersection point corresponding to critical sill flow in Figure 1.9.1a. For the (non-conservative) solutions shown in Figure 1.10.5 or 1.10.6, an intersection implies only that the depths of the two solutions are equal, not necessarily the fluxes or values of g'. For example the intersection between the dashed curves near x=-1.9 in Figure 1.10.5a involves two solutions with identical depths but different Froude numbers (as shown in the Figure 1.10.5b).

The previous case involved v_1=0, so entrainment occurred only when the flow was supercritical. One consequence is that critical flow can only occur at the sill. We next consider a case with finite upper velocity, v_1=-1 (Figure 1.10.6). A reverse upper layer velocity is characteristic of outflows from marginal seas, a subject treated in Chapter 5. Inspection of Figure 1.10.6a shows that critical transitions occur downstream of the sill as predicted by (1.10.8). As in the previous case, entrainment tends to push the solutions towards a critical state (Figure 1.10.6b) and, in the case of some of the supercritical curves, results in the formation of an infinite interface slope corresponding to a hydraulic jump. Jumps are represented in the figure by vertical terminations of the dashed curves.

One of the strongest assumptions made in connection with entraining layer models is that density and momentum carried across an interface are instantly mixed over the thickness of the target layer. In reality this mixing is rarely complete and the resulting distribution of v and ρ within the layer are vertically non-uniform. One of the most striking example is the exchange flow in the Strait of Gibraltar (Figure I9) where mixing between the inflowing and outflowing layers is confined to a relatively thin interfacial layer. In the Bab al Mandab (Figure 1.10.7) the interfacial region is much thicker, but v and ρ remain strongly non-uniform. Further discussion of this subject can be found in Nielsen *et al.* (2004).

Exercises:

1) For the case of entrainment with no bottom friction or variations in w and h, derive an equation for the rate of change of d_2 with y (comparable to 1.19.12). For subcritical flow, comment on possible circumstances in which d_2 can increase while F increases.

Figure Captions

1.10.1 Continuously stratified exchange flow as computed by a nonhydrostatic, two-dimensional model. The upper panel shows the stratification in terms of g'/g_o', where $g' = g(\rho(y,z)-\rho_1)/\rho_1$, ρ_1 is the density of the overlying fluid, and g_o' is the upstream value of g' based on the two homogeneous layers there. The middle panel shows contours of horizontal velocity while the lower panel shows the streamlines. Other scales include the half length L of the obstacle and the height h_m of the obstacle. (From Nielsen, 2004).

1.10.2 (a): The intermediate layer formed due to interfacial instability and mixing between two layers of different density moving at different speeds. (b): An idealization of the flow in which all fluid below the top of the mixing wedge in (a) is considered to be a single layer and where the transfer of mass into that layer is represented by an entrainment velocity w_e.

1.10.3 The control volume used as a basis for mass and momentum budgets for the lower layer.

1.10.4 Entrainment coefficient w_e/V as a function of Froude number. The entrainment velocity is directed normal to the bottom and V represents the velocity parallel to the bottom and δV is the jump in V across the interface. The Froude number is based on this δV and on the layer thickness measured normal to the bottom. Data from laboratory experiments of Ellison and Turner (1959), Alavian (1986) and Cenedese *et al.* (2004) are indicated, as are observations in the Mediterranean, Denmark Strait and Faroe-Bank Channel (all from Baringer and Price, 1999), and from Lake Ogawarra (Dillimore *et al.* 2001). The Princevac *et al.* data are from an atmospheric gravity current with higher Reynolds numbers than the ocean and laboratory examples. (Based on a figure from Wells and Wettlaufer 2005 and on M. Wells and J. Price, *private communications*.)

1.10.5 A family of steady solutions, all having the same upstream values of volume flux and g' but different lower layer thicknesses. Entrainment is parameterized using the Ellison-Turner formulation (1.10.9) and the velocity v_1 in the overlying fluid is zero. The z-coordinate in the upper panel has been normalized using the obstacle height and the obstacle height-to-length ratio is 0.2. The lower panel shows the Froude numbers. L and h_m are the obstacle half width and height. (From Nielsen, et al. 2004.)

1.10.6 Same as Figure 1.10.5 except that the upper layer velocity is negative, in this case $v_1/(g'h_m)$=-1. (Frim Nielsen et al. 2004).

1.10.7 A temperature section along the central axis of the Bab al Mandab, with the Red Sea to the left. (Courtesy of Dr. S. Murray).

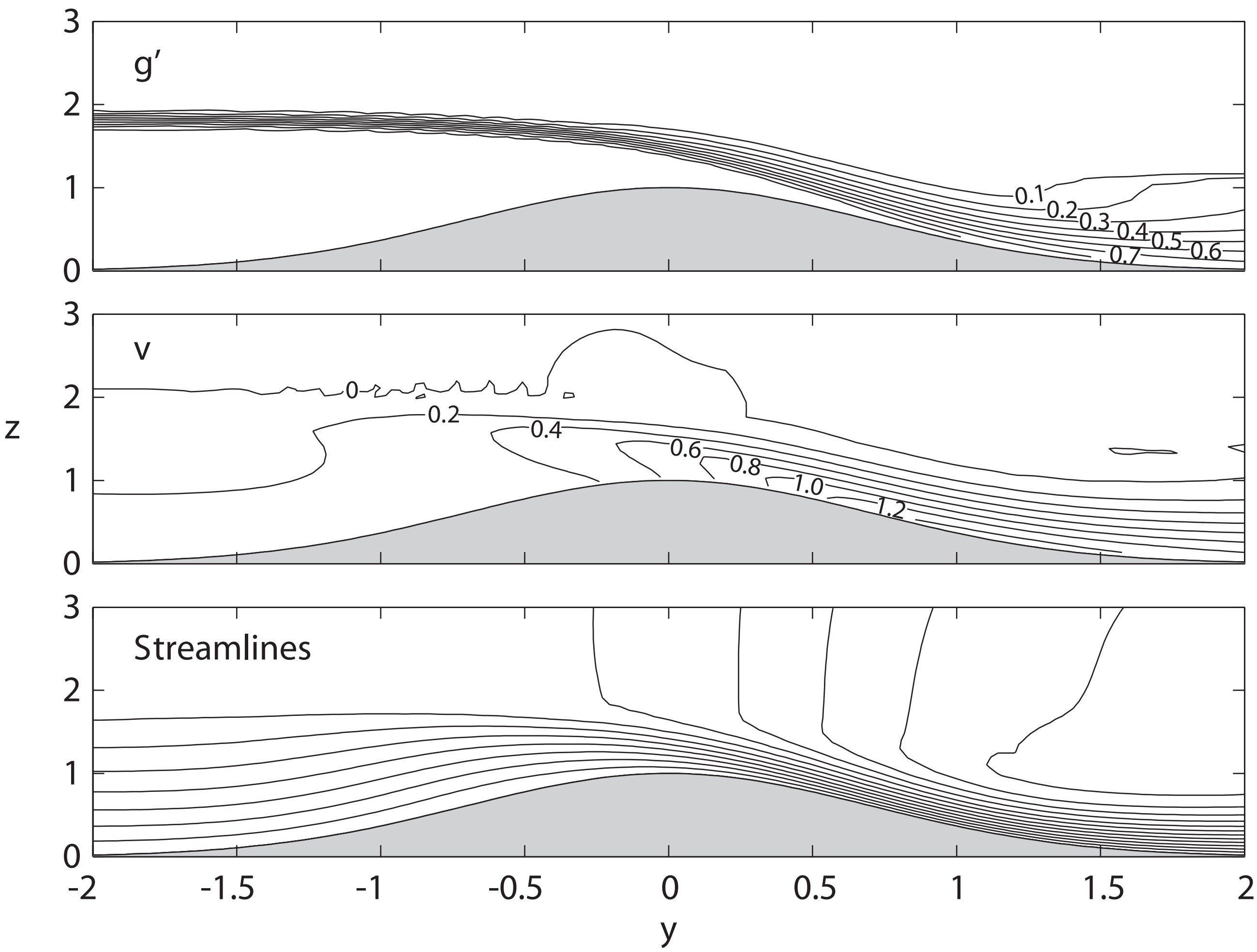
g′
0.1
0.2
0.3
0.4
0.5
0.6
0.7
v
0
0.2
0.4
0.6
0.8
1.0
1.2
Streamlines
z
y
3
2
1
0
-2
-1.5
-1
-0.5
0
0.5
1
1.5
2

Figure 1.10.1

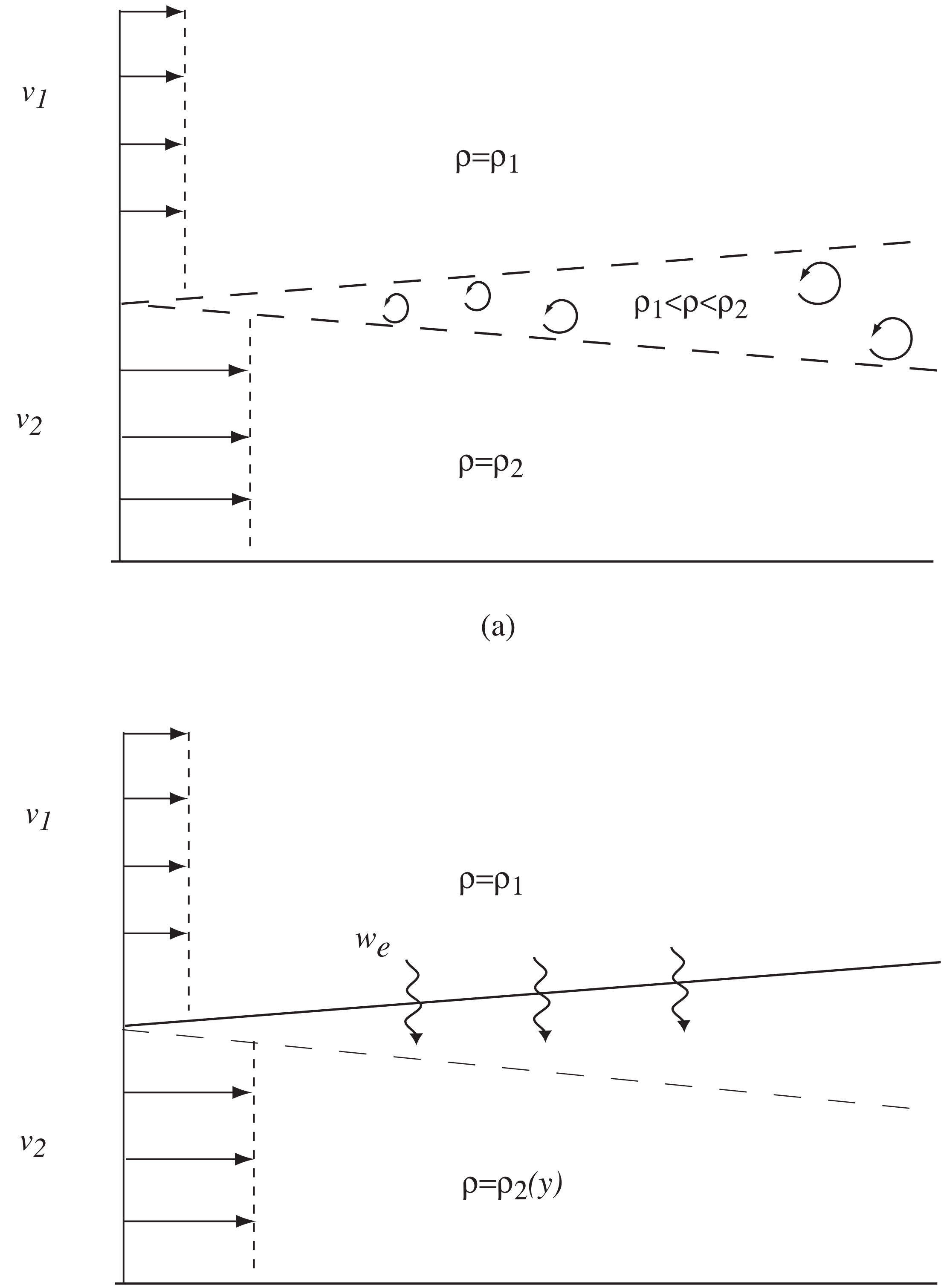
v_1
$\rho=\rho_1$
$\rho_1<\rho<\rho_2$
v_2
$\rho=\rho_2$
(a)
v_1
$\rho=\rho_1$
w_e
v_2
$\rho=\rho_2(y)$
(b)

Figure 1.10.2

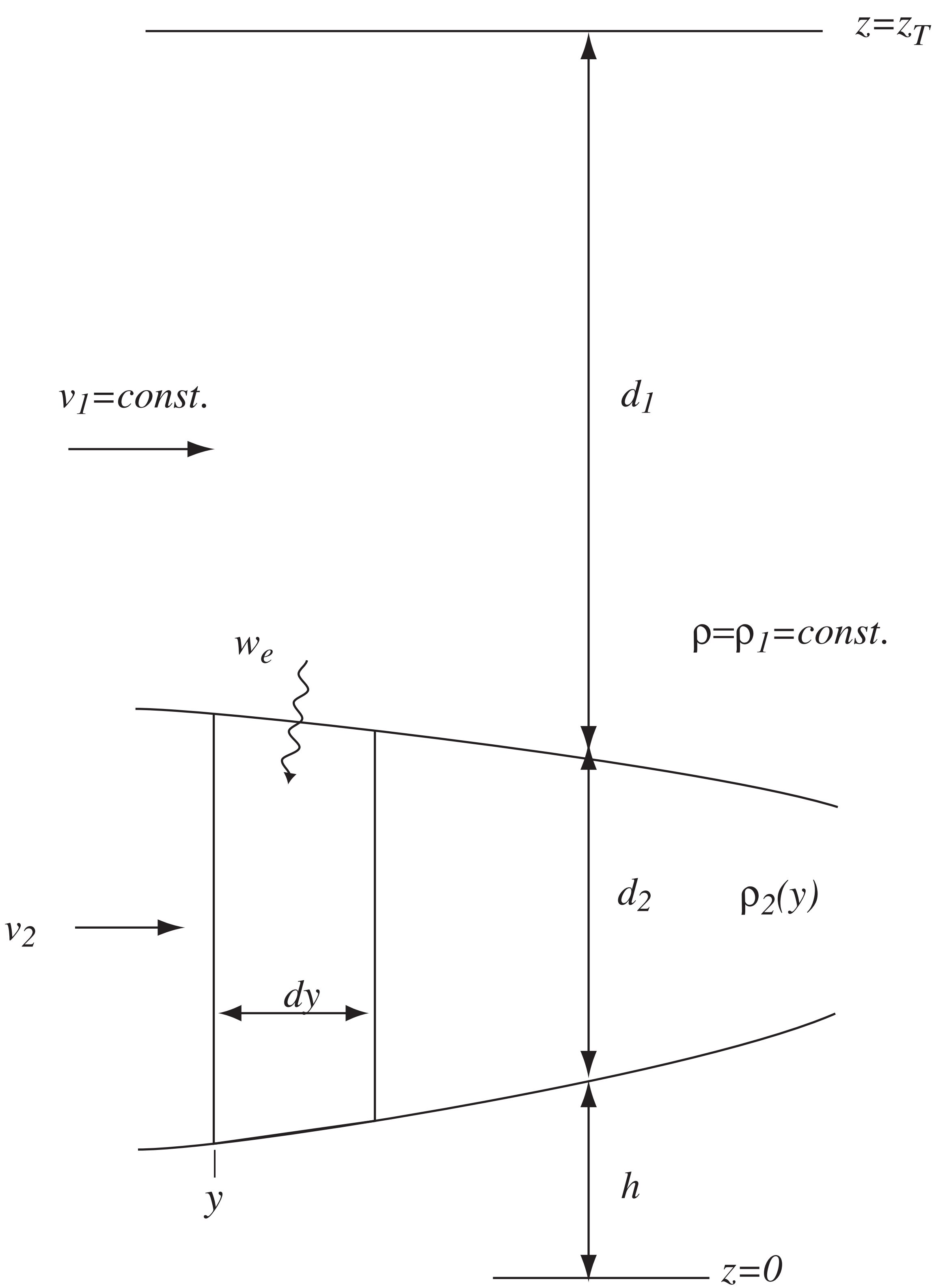

Figure 1.10.3

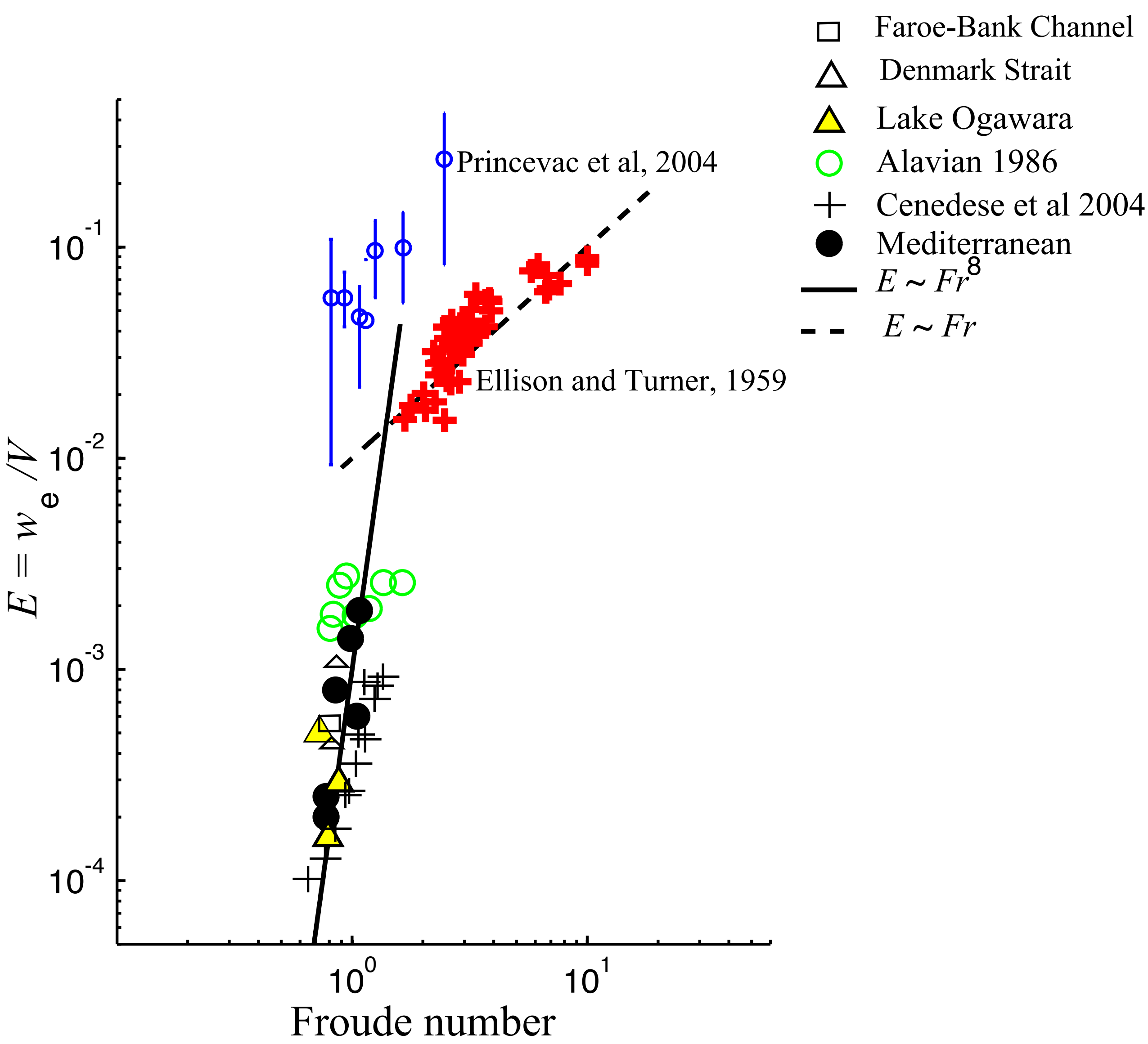

Faroe-Bank Channel
Denmark Strait
Lake Ogawara
Alavian 1986
Cenedese et al 2004
Mediterranean
$E \sim Fr^8$
$E \sim Fr$
Princevac et al, 2004
Ellison and Turner, 1959
$E = w_e/V$
Froude number

Figure 1.10.4

(a)

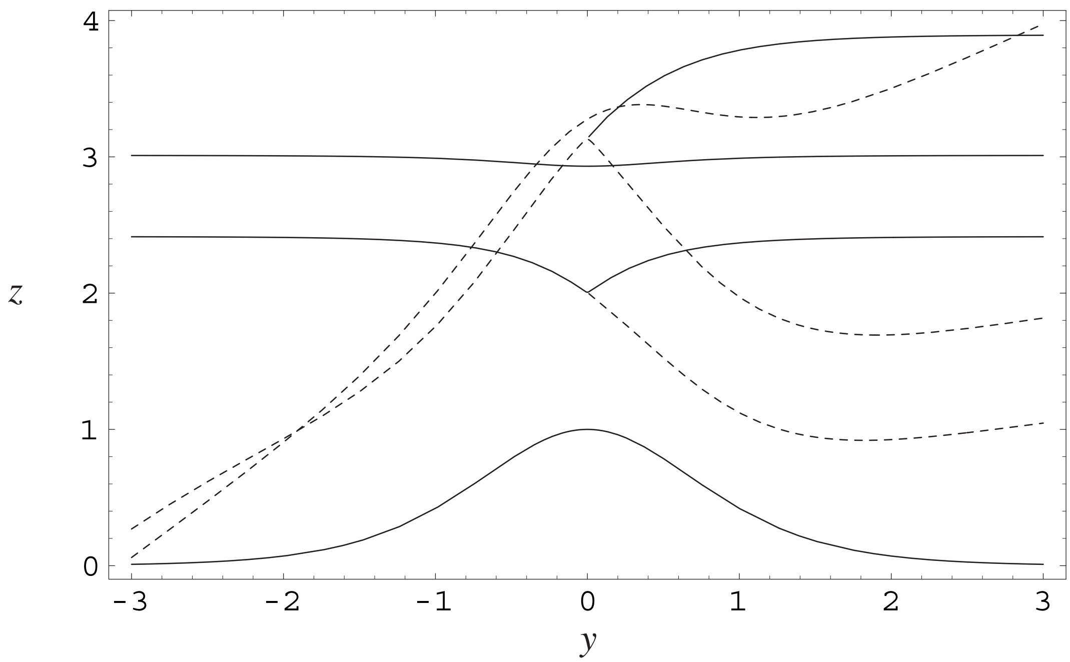

(b)

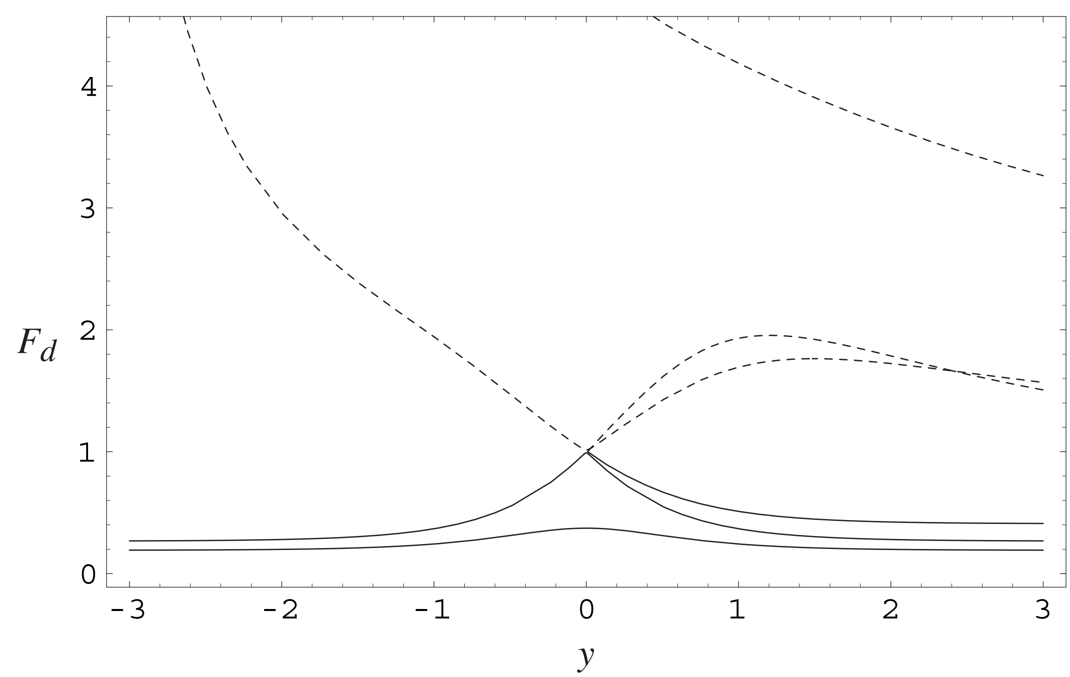

Figure 1.10.5

(a)

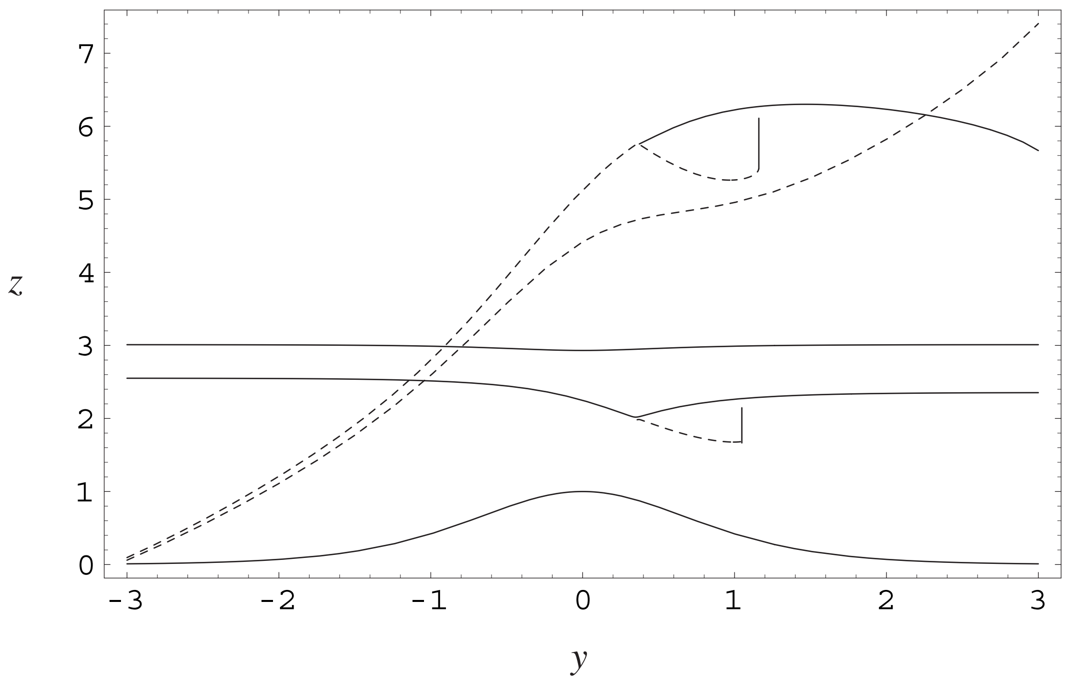

(b)

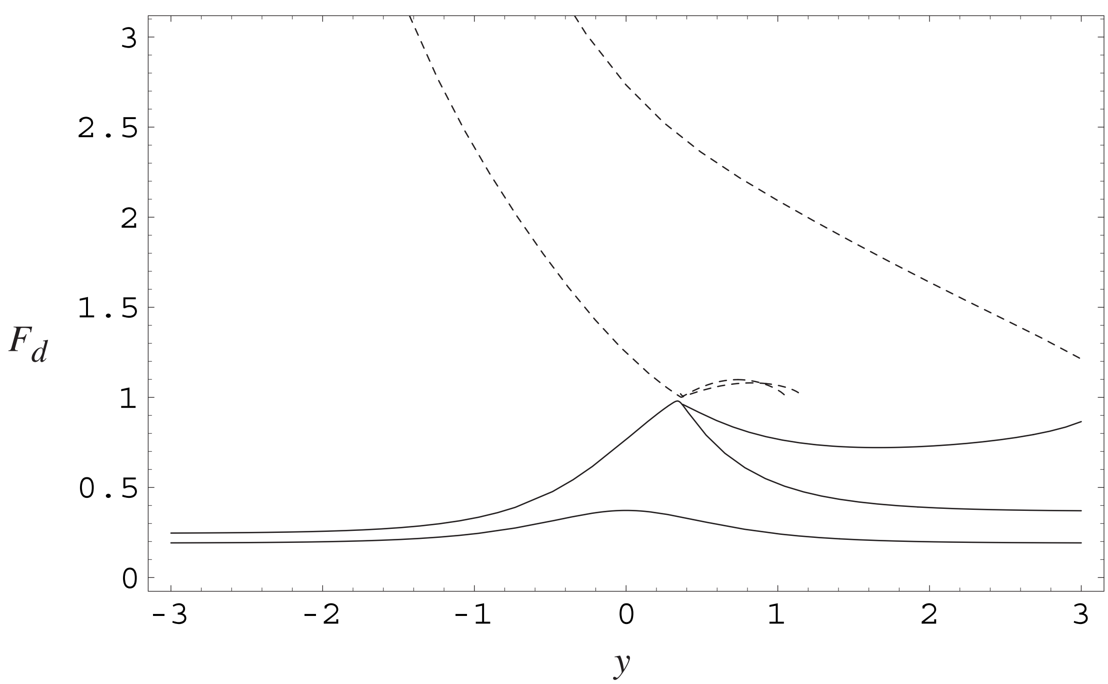

Figure 1.10.6

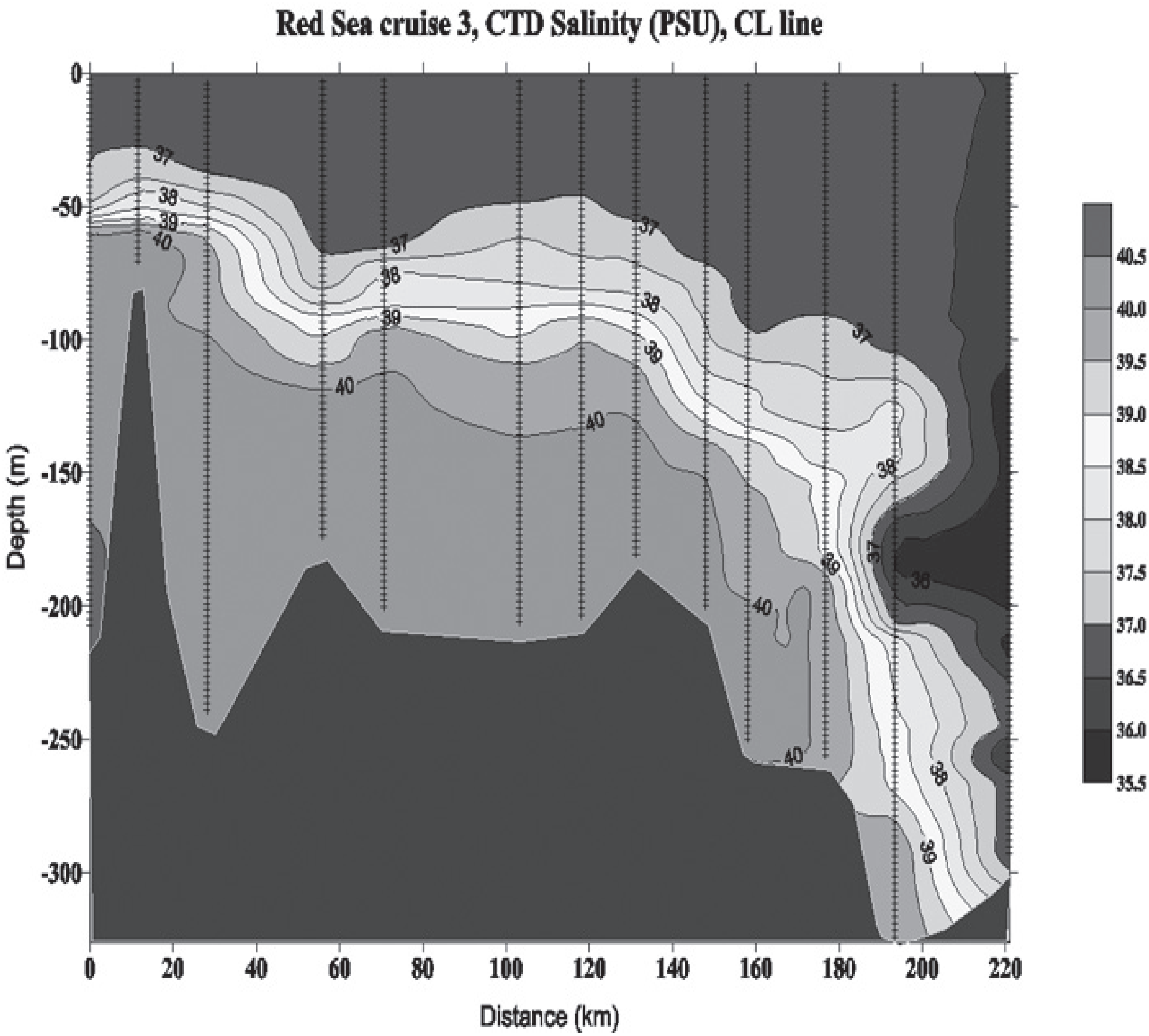
Red Sea cruise 3, CTD Salinity (PSU), CL line
Depth (m)
Distance (km)
0
-50
-100
-150
-200
-250
-300
0
20
40
60
80
100
120
140
160
180
200
220
40.5
40.0
39.5
39.0
38.5
38.0
37.5
37.0
36.5
36.0
35.5

Figure 1.10.7